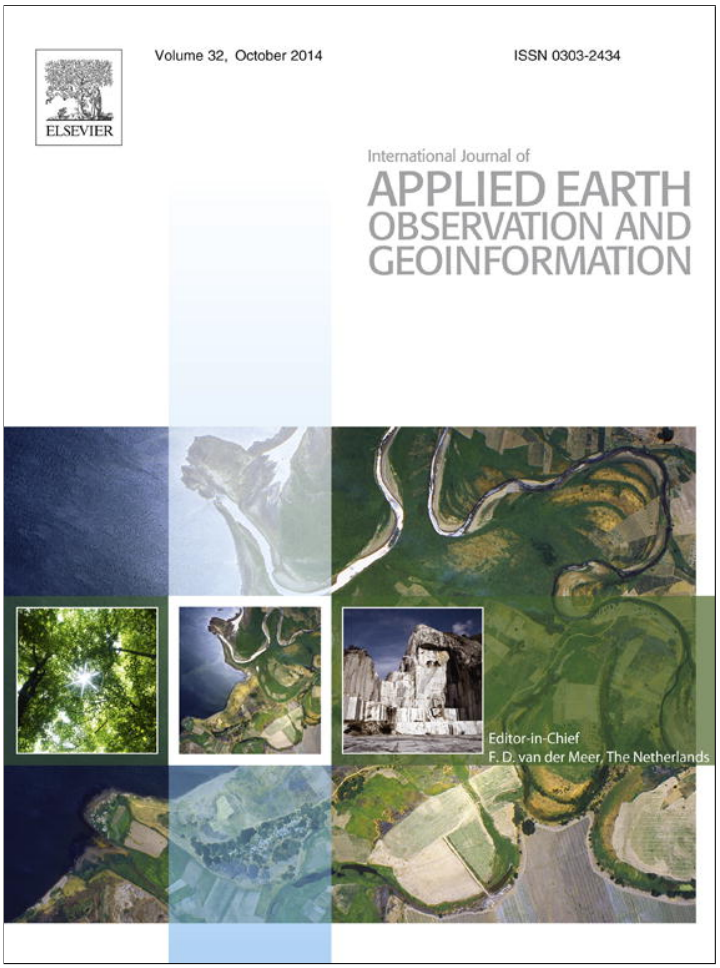

International Journal of Applied Earth Observation and Geoinformation 32 (2014) 54–66

Contents lists available at ScienceDirect

International Journal of Applied Earth Observation and Geoinformation

journal homepage: www.elsevier.com/locate/jag

# Estimating the spatial distribution of soil moisture based on Bayesian maximum entropy method with auxiliary data from remote sensing

Shengguo Gao[a,b], Zhongli Zhu[a,b,*], Shaomin Liu[a,b], Rui Jin[c], Guangchao Yang[a,b], Lei Tan[a,b]

[a] School of Geography, Beijing Normal University, Beijing 100875, China
[b] State Key Laboratory of Remote Sensing Science, Jointly Sponsored by Beijing Normal University and Institute of Remote Sensing and Digital Earth Chinese Academy of Sciences, Beijing 100875, China
[c] Cold and Arid Regions Environmental and Engineering Research Institute, Chinese Academy of Sciences, Lanzhou 730000, China

ARTICLE INFO

*Article history:*
Received 28 August 2013
Accepted 10 March 2014
Available online 23 April 2014

*Keywords:*
Soil moisture
Remote sensing
Wireless sensor network (WSN)
Bayesian maximum entropy (BME)
Soft data

ABSTRACT

Soil moisture (SM) plays a fundamental role in the land–atmosphere exchange process. Spatial estimation based on multi in situ (network) data is a critical way to understand the spatial structure and variation of land surface soil moisture. Theoretically, integrating densely sampled auxiliary data spatially correlated with soil moisture into the procedure of spatial estimation can improve its accuracy. In this study, we present a novel approach to estimate the spatial pattern of soil moisture by using the BME method based on wireless sensor network data and auxiliary information from ASTER (Terra) land surface temperature measurements. For comparison, three traditional geostatistic methods were also applied: ordinary kriging (OK), which used the wireless sensor network data only, regression kriging (RK) and ordinary co-kriging (Co-OK) which both integrated the ASTER land surface temperature as a covariate. In Co-OK, LST was linearly contained in the estimator, in RK, estimator is expressed as the sum of the regression estimate and the kriged estimate of the spatially correlated residual, but in BME, the ASTER land surface temperature was first retrieved as soil moisture based on the linear regression, then, the *t*-distributed prediction interval (PI) of soil moisture was estimated and used as soft data in probability form. The results indicate that all three methods provide reasonable estimations. Co-OK, RK and BME can provide a more accurate spatial estimation by integrating the auxiliary information Compared to OK. RK and BME shows more obvious improvement compared to Co-OK, and even BME can perform slightly better than RK. The inherent issue of spatial estimation (overestimation in the range of low values and underestimation in the range of high values) can also be further improved in both RK and BME. We can conclude that integrating auxiliary data into spatial estimation can indeed improve the accuracy, BME and RK take better advantage of the auxiliary information compared to Co-OK, and BME outperforms RK by integrating the auxiliary data in a probability form.



## Introduction

Soil moisture (SM) plays a fundamental role in the land–atmosphere exchange process because it controls both evaporation from bare soil and transpiration from vegetated areas. Many scientific studies and applications require global, continental or regional soil moisture data to represent the initial state for the soil moisture variables, just like forecasts of weather variations, models of plant growth and carbon flux and models of land surface hydrological processes etc. A number of studies have been conducted to obtain soil moisture estimates from various observations and models (Vereecken et al., 2008; Wang and Qu, 2009; Guswa et al., 2002), but more often, the large spatial–temporal variation results in very uncertain estimation. Obtaining accurate soil wetness information by remote sensing techniques has great potential and is the focus of ongoing research, especially after the operation of the Soil Moisture and Ocean Salinity (SMOS) (Kerr et al., 2010), Aquarius (Le Vine et al., 2010), and the launch of Soil Moisture Active Passive (SMAP) in future (Entekhabi et al., 2010). Monitoring land surface soil moisture by ground-based techniques can also be valuable, for drought monitoring, precision agriculture, and especially for the validation of remote sensing soil moisture

* Corresponding author at: School of Geography, Beijing Normal University, No. 19, Xinjiekouwaida Street, Haidian District, Beijing 100875, China. Tel.: +86 010 58806902; fax: +86 010 58805274.
*E-mail address:* bnufuture@126.com (Z. Zhu).

http://dx.doi.org/10.1016/j.jag.2014.03.003
0303-2434/

products (Jackson et al., 2009, 2011). With the development of wireless communication techniques, the wireless sensor network (WSN) has been increasingly used in eco-hydrological monitoring (Akyildiz et al., 2002; Ruiz-Garcia et al., 2009). This technology makes it possible to take simultaneous measurements of regional soil moisture, unlike conventional ground-based methods (Bogena et al., 2010).

Soil moisture information from WSN can be regarded as a multi-point simultaneous survey. To understand the spatial distribution and variation of soil moisture or to compare it to remote sensing products, we need to estimate the soil moisture distribution map or up-scale to a certain scale. Traditional geostatistics, such as kriging, is a powerful interpolation tool that quantifies and reduces the uncertainties of estimation and minimizes investigation costs, and has been used to provide linear unbiased predictions at unsampled locations for over four decades (Burgess and Webster, 1980; Cressie, 1990). The estimation accuracy of the kriging method is usually limited by the density and distribution of sample sites. Theoretically, if additional covariates which are spatially correlated with soil moisture and more easily or intensively sampled are integrated into the estimator, the estimation accuracy may be improved. Spatial estimation methods (such as co-kriging, regression kriging, and universal kriging, et al.) that account for covariates could play an important role here. These methods could conceivably result in a considerable reduction of costs while achieving a comparable degree of accuracy by using fewer relatively expensive variables and more relatively inexpensive covariates (Stein et al., 1988; Stein and Corsten, 1991; Zhang et al., 1992, 1997; Wu et al., 2003), especially in the under-sampled cases (Yates and Warrick, 1987). Universal kriging and regression kriging differ in the computational steps, however, the resulting predictions and prediction variances are the same. Co-kriging (Co-OK) is mainly developed for situations in which the auxiliary information is not spatially exhaustive (Knotters et al., 1995), in cases where the covariates are available as maps, regression kriging (RK) will generally be preferred over Co-OK, although Co-OK may in some circumstances give superior results (Asli and Marcotte, 1995; Goovaerts, 1999; Rivero et al., 2007; Moral, 2010; Hernández-Stefanoni et al., 2011). Studies have also demonstrated that Co-OK is only minimally superior to ordinary kriging when the auxiliary variables are not highly correlated with object variables (Asli and Marcotte, 1995; Triantafilis et al., 2001; Wu et al., 2009), and in some cases, the covariates were of little significance for prediction due to underweighting (the weights of covariates sum to zero and are often of small magnitude) (Goovaerts, 1998). Thus, different methods that may fit certain situations better. New methods are needed in spatial estimation of soil moisture which can incorporate auxiliary data of different origin and reliability in a systematic and rigorous way.

Bayesian maximum entropy (BME) (Christakos, 1990a, 1990b, 1991, 2000), which belongs to the field of modern spatiotemporal geostatistics, provides a systematic and rigorous approach for integrating physical knowledge into spatiotemporal analysis, including statistical moments of any order, physical laws, scientific theories, empirical relationships, and uncertain observations (Christakos and Serre, 2000; Christakos et al., 2001). As a significant generalization of commonly used geostatistical techniques, it does not make the Gaussian distribution hypothesis, and it can estimate variables by non-linear prediction (Christakos, 1990a; Christakos and Li, 1998). In the two decades since its initial proposal, BME has been successfully used in many research fields. In the field of environment and public health, the PM10 distribution in the state of North Carolina was studied by using the Bayesian maximum entropy (BME) mapping method (Christakos and Serre, 2000). Another study focused on the spatiotemporal distribution of ozone (Yu et al., 2009; Bogaert et al., 2009). BME can readily consider uncertain yet valuable information at the estimation points. Additionally, in the framework of BME, good estimates of childhood asthma prevalence at fine spatial resolution were obtained by nonlinear integration of prevalence data aggregated over large areas and the data obtained at the fine scale of interest (Lee, 2005; Lee et al., 2009). In the field of soil science, D'Or et al. (2001) and D'Or (2003) investigated the use of BME for estimating soil textural fractions in space by integrating a small hard data set with a larger soft data set. The results show that BME is more accurate than simple kriging estimates, thus offing a better picture of the soil reality. Similarly, in Bogaert and D'Or (2002), the thematic maps and the data from laboratory analysis were incorporated into BME to obtain a more accurate estimation map of soil texture. BME illustrates the advantages of using soft information on a sound theoretical basis. Additionally, as one of the spatiotemporal knowledge synthesis and mapping methods, BME has been successfully applied in the data fusing field for the fusing of observations and model predictions (Christakos et al., 2004; Nazelle et al., 2010) or multi-sensors data (Li et al., 2012, 2013a,b). Only a fraction of the possible applications are listed above, but this list still shows that BME performs wonderfully in the field of spatial (or spatiotemporal) estimation, especially for the fusing of uncertain auxiliary information. BME has also been shown to be more accurate and physically meaningful than classical geostatistics (e.g., Christakos and Li, 1998; Serre and Christakos, 1999; Douaik et al., 2004; Pang et al., 2010). In this study, we attempt to introduce BME as a spatial estimator of soil moisture.

In the ground ecosystem, both land surface soil moisture and land surface temperature (LST) vary spatially due to soil type, land cover, and land use, and they vary temporally with the time of day and the season of the year. Studies show that the LST maximum during moist conditions occurs later in the day than during dry conditions, and land surface soil moisture and LST have been found to be negatively correlated (Lakshmi et al., 2000; Sun and Pinker, 2004), which indicates that valuable information about the spatial distribution of soil moisture can be obtained from the LST. The purpose of this study is to present a novel approach to estimate the spatial pattern of soil moisture by using BME method based on wireless sensor network data and the auxiliary information from ASTER (Terra) LST. For comparison, traditional geostatistic methods were also applied: ordinary kriging (OK), co-kriging (Co-OK) and regression kriging (RK).

## Materials and methods

### *Study area and soil moisture wireless sensor network*

The experimental area involved in this study (Fig. 1) was located in the Zhangye artificial oasis in the middle reaches of the Heihe River Basin (HRB) in northwestern China (38.871° N, 100.359° E). As a typical inland river basin characterized by distinct cold and arid landscapes distributed upstream to downstream, the HRB has long served as a test bed for integrated watershed studies and hydrological experiments (Cheng, 2009). Comprehensive experiments such as HEIFE (Hu et al., 1994) and WATER (Li et al., 2009) have taken place in the HRB, and HiWATER (Li et al., 2013a,b) is still in progress. The soil moisture wireless sensor network (WATERNET) shown in Fig. 1 was part of the first thematic experiment of HiWATER, which is referred to as Multi-Scale Observation Experiment on Evapotranspiration over heterogeneous land surfaces 2012 (MUSOEXE-12). The experiment included two nested matrixes: one large experimental area (composed of oasis and desert) covering an area of 30 km × 30 km and one kernel experimental area (completely in the oasis) covering 5.5 km × 5.5 km. WATERNET was located in the kernel experimental area, and the observations lasted from May 2012 to September 2012. The

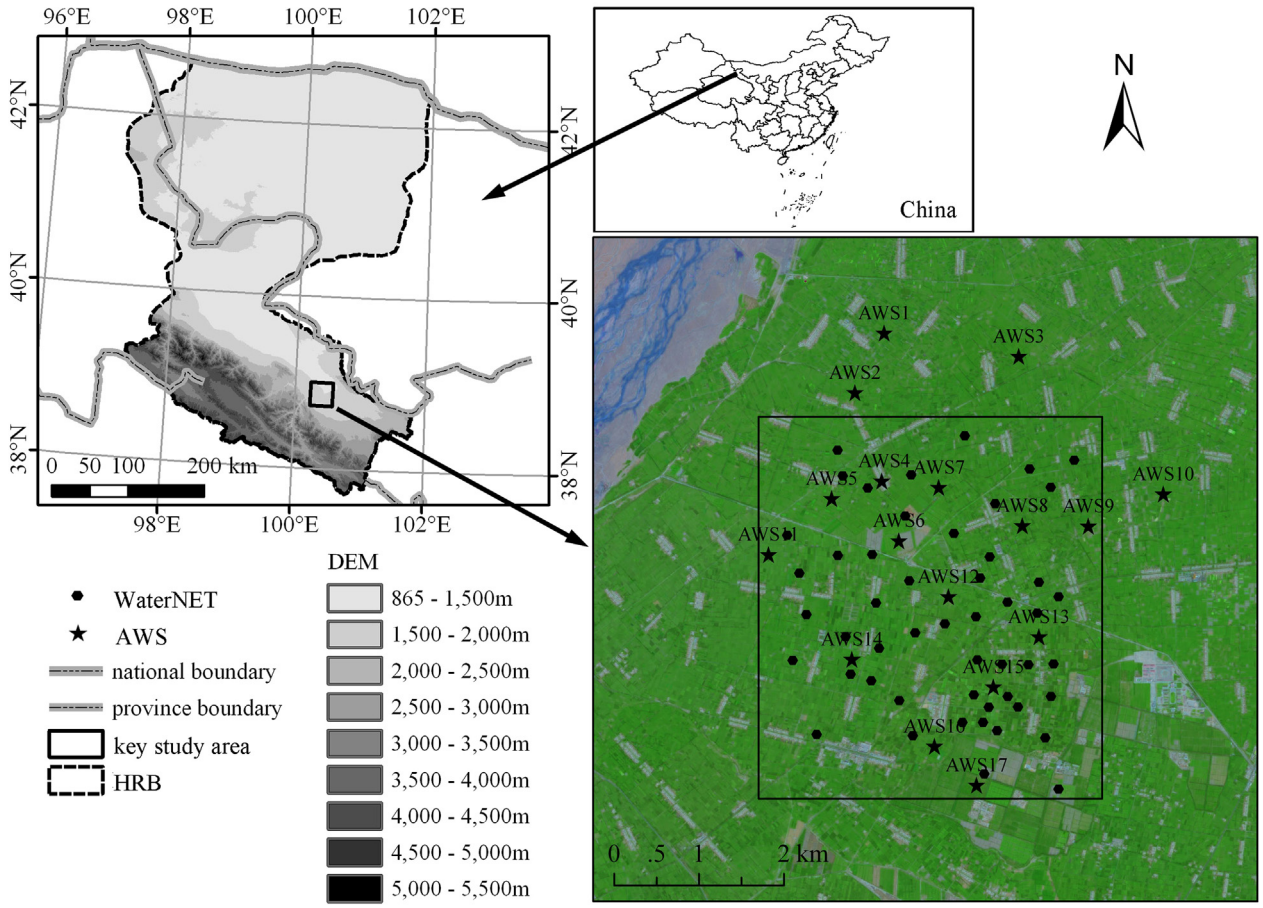


**Fig. 1.** Overview of the study area. The sub-image in the upper left corner is the DEM of HRB. The sub-image in the lower right corner is the true color image of SPOT covering the key study area.

precipitation in the Zhangye oasis is approximately 100–250 mm per year. Irrigation is the main water source. The potential evaporation is as high as 1200–1800 mm per year (Li et al., 2013a,b). The major crops there are maize, wheat, and vegetables. In this study, we chose the approximately 4.5 km × 5.0 km area covered by WATERNET as the key study area (Fig. 1). WATERNET consists of 50 nodes, and each node includes soil moisture and soil temperature observations for two layers (4 cm, 10 cm). The measurements of soil moisture are based on the frequency-domain reflectometry method using a Hydro Probe II (HP-II) sensor. The design of WATERNET, the data communication style and other information can be found in Jin et al. (2012). In the key study area, there are also thirteen Auto Weather Stations (AWS), as shown in Fig. 1. All of the AWS except AWS4 (in the underlying of village) include the soil moisture observations at a depth of 4 cm. The soil moisture sensors for AWS12, AWS13, and AWS14 are $ECH_2O$-5 (Decagon Device). For the left AWS, the sensors are CS616 (Campbell). Comparative work was carried out before the installation of all the soil moisture sensors in the field. The results show that the Hydra Probe II has a mean underestimation of 0.025 $m^3/m^3$ compared with the gravimetric method for the saturated soil. CS616 gives an overestimation of 0.035, and $ECH_2O$-5 has an underestimation of 0.085. In dry soil, the observation values of the three sensors were all less than 0.02 $m^3/m^3$. All of the soil moisture data used in this study was linearly calibrated based on the comparative data.

*Data summary*

In this study, WSN data from the following three periods were used: May 30, 2012; June 15, 2012; and June 24, 2012. ASTER (Terra) image data were available for each period, and some of the AWSs had already started to run normally at these times. At these three stages, the study area still exhibited sparse vegetation cover, and the land surface wetness and land surface temperature (LST) showed an obvious negative correlation. Therefore, the LST retrieved from ASTER can be properly regarded as auxiliary information in the spatial estimation of soil moisture. With regard to the WSN data, we used the daily mean soil moisture at 4 cm depth and assumed that the WSN observations were sufficiently accurate to be considered as hard data. The ASTER LST used here was retrieved by the radiative transfer equation method (Ottlé and Stoll, 1993; Zhou et al., 2012). In BME, ASTER LST was retrieved as soil moisture

**Table 1**
Summary of WSN data used in the study.

| Date | Data | No. | Max (%) | Min (%) | Range (%) | Mean (%) | SD (%) |
|---|---|---|---|---|---|---|---|
| May 30, 2012 | SM (WATERNET) | 47 | 38 | 6 | 32 | 18 | 7.38 |
| June 15, 2012 | SM (WATERNET) | 45 | 32 | 13 | 20 | 23 | 4.25 |
| June 24, 2012 | SM (WATERNET) | 42 | 41 | 11 | 30 | 20 | 7.13 |

*Note*: Units for max, min, range, mean, SD are $m^3/m^3$.

**Table 2**
Summary of ASTER LST data used in the study.

| Date | Data | Area | Max (K) | Min (K) | Range (K) | Mean (K) | SD (K) |
|---|---|---|---|---|---|---|---|
| May 30, 2012 | LST (ASTER) | 50 × 55 (90 m) | 324.08 | 298.14 | 25.94 | 314.55 | 5.84 |
| June 15, 2012 | LST (ASTER) | 50 × 55 (90 m) | 314.65 | 298.34 | 16.31 | 306.05 | 2.09 |
| June 24, 2012 | LST (ASTER) | 50 × 55 (90 m) | 313.19 | 295.85 | 17.34 | 302.66 | 2.88 |

that was expressed as soft data in probability form. The creation of soft data will be discussed in Section "Preparation of soft data". Tables 1 and 2 provide the summary statistics of the WSN data and the ASTER LST. Because of maintenance mistakes, only 47 of the 50 WSN nodes had normal observations on May 30. Likewise, there were 45 good nodes on June 15 and 42 good nodes on June 24. In this study, relative to the study area of 4.5 km × 5 km and the study resolution of 90 m (a total of approximately 2500 pixels), the hard data here should be considered an under-sampled case (Bartlett et al., 2001). As shown in Table 1, the soil moisture on May 30 had the lowest relative mean value but the largest standard derivation (SD) among the three periods. These data indicate that the study area on May 30 was in the driest of the three stages but had large spatial variation. Table 2 shows similar statistical characteristics for the LST. It should be noted that the indices in Table 2 are the statistical results of non-building pixels. The area of building in the ASTER LST has been masked because it would introduce incorrect reference information as the auxiliary data in the spatial estimation of soil moisture based on spatial correlation.

### *Preparation of soft data*

Including soft data in BME is an important way to integrate uncertain information into the estimation. Properly expressed soft data can enhance the value of uncertain information. Soft data can be incomplete and/or qualitative observation statements linked to experts' opinions, experiences, intuition, questionnaires, equipment shortcomings, etc. (Christakos et al., 2002). Probability and interval soft data, in particular, are very common in real practice. Probability soft data can be the result of measurement error, physical interpretation, etc., and they are approximately normally distributed or Student's $t$-distributed (Christakos and Li, 1998; Christakos et al., 2001). Interval soft data with upper and lower bounds do not fit a probability distribution but do have physical meanings (Douaik et al., 2005). In this study, a probability statement was used and expressed as Student's $t$-distributed data by estimating the prediction interval (PI) of linear regression. Eq. (1) shows the empirical linear relationship between SM ($\hat{P}$) and LST ($T$). We can estimate the PI according to Eq. (2) (Younger, 1985):

$$\hat{P} = aT + b \tag{1}$$

$$P_{\text{interval}} = \hat{P}_i \pm t_{n-2,0.025} S_{T\cdot P} \sqrt{1 + \frac{1}{n} + \frac{(T_i - \bar{T})^2}{S_{TT}}} \tag{2}$$

Here, $Y_{\text{interval}}$ is the PI corresponding to each estimated soil moisture $\hat{P}_i$ relative to the land surface temperature $T_i$, is the sample size of the regression, $t_{n-2,0.025}$ is the critical value of the t-distribution with degrees of freedom of $(n-2)$ and a confidence level of 95%, $S_{T\cdot P}$ is the standard deviation of the regression error, $\bar{T}$ is the mean value of the land surface temperature, and $S_{TT}$ is the sum of the square of the deviations. SM of WSN and the corresponding nearest pixel value of the ASTER LST are used to obtain the fitted relationship shown in Eq. (1). The regression correlation coefficients (in Table 3) show moderate correlation between SM of WSN and ASTER LST in the study area. By using Eqs. (1) and (2), LST can be expressed as probability soft data. Fig. 2 shows the SM-LST linear relationship, the corresponding PI and the probability distribution at the specified LST in each period. All of the parameters for the three dates involved in Eqs. (1) and (2) can be found in Table 3.

### *Methods*

As mentioned above, four spatial estimation methods were involved in this study. Here, only an outline of these methods is given; in-depth discussions can be found in the references cited. The performances of these methods were evaluated by using a cross-validation (leave-one-out) method and an absolute validation method introduced later.

#### *Variogram and cross-variogram*

The variogram and cross-variogram contain spatial correlation information, and they are the main components of geostatistical methods. Assuming the intrinsic hypothesis, the following function gives a measure of how well a random variable is correlated in space as a function of separation distance in the case of two variables (Yates and Warrick, 1987; Boyer et al., 1996):

$$\gamma_{ij}(h) = \frac{1}{2N} \sum_{k=1}^{N(h)} \{[Z_i(v_k + h) - Z_i(v_k)][Z_j(V_k + h) - Z_j(V_k)]\} \tag{3}$$

Here, $V_k$ denotes the spatial location of the sample, $\gamma_{i,j}$ indicates the semivariance (when $i=j$) with respect to the random variable $Z_i$ at a separation distance $h$ and $N(h)$ is the number of pairs of $Z_i(V_k)$ and $Z_j(V_k)$ in a given lagged distance interval $(h+dh)$. When $i \neq j$, $\gamma_{i,j}$ is the cross-semivariance as a function of $h$. In the case of the cross-variogram, the semivariance of two variables and the cross-semivariance must satisfy the Cauchy-Schwartz inequality: $|\gamma_{ij}(h)| \leq |\gamma_{ii}(h)\gamma_{jj}(h)|^{1/2}$ (Yates and Warrick, 1987). In this study, two nested variogram models were used. Model (1) is a nugget-exponential model (Eq. (4)), and model (2) is a nugget-spherical model (Eq. (5)) (Zhang, 2005):

$$\gamma(h) = C_0 + C_1 \left(1 - e^{\frac{3h}{a}}\right) \tag{4}$$

$$\gamma(h) = \begin{cases} C_0 + C_1 \left[1.5\left(\frac{h}{a}\right) - 0.5\left(\frac{h}{a}\right)^3\right], & 0 \leq h \leq a \\ C_0 + C_1 & h > a \end{cases} \tag{5}$$

**Table 3**
Parameters of the linear regression and summary statistics of the soft data.

| Date | Model | CR | $a$ | $b$ | $R^2$ | $\bar{X}$ | $S_{XX}$ | $S_{XY}$ | $n$ | $t_{n-2,0.025}$ |
|---|---|---|---|---|---|---|---|---|---|---|
| May 30 | Linear | 0.66 | −0.94 | 318.00 | 0.44 | 316.79 | 1232.07 | 5.59 | 47 | 2.0141 |
| June 15 | Linear | 0.53 | −1.08 | 351.45 | 0.28 | 306.05 | 190.73 | 3.61 | 45 | 2.0167 |
| June 24 | Linear | 0.59 | −1.64 | 517.06 | 0.35 | 303.44 | 279.94 | 5.67 | 43 | 2.0195 |

*Note*: CR, coefficient of correlation; $a$, $b$, parameters of linear regression; $R^2$, coefficient of determination. Others are the same to variables in Eq. (2).

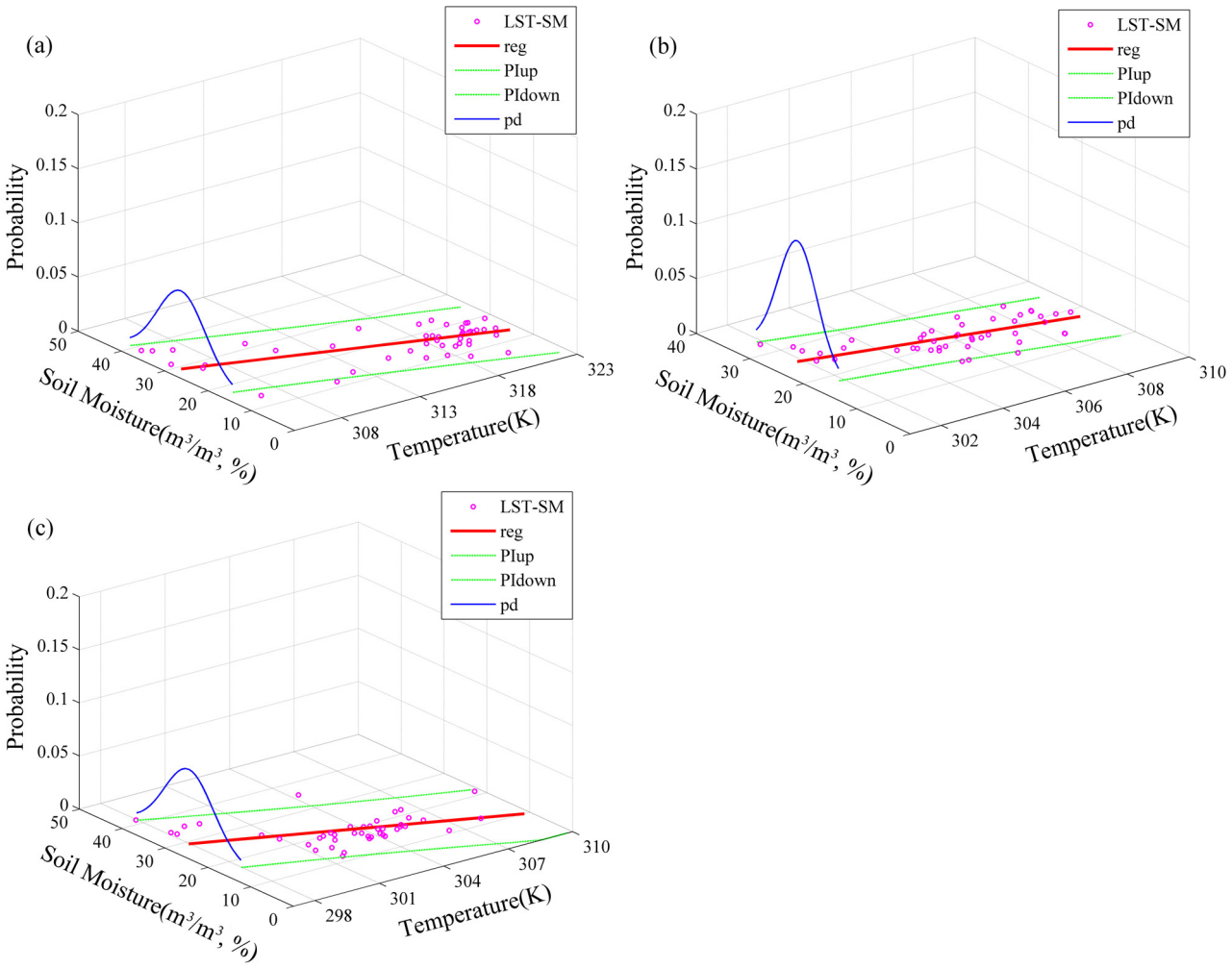


**Fig. 2.** SM-LST scatters plots, linear regression and the scheme of probability soft data. (a)–(c) are shown separately for May 30, 2012, June 15, 2012 and June 30, 2012. The red line (reg in the legend) indicates the regression line. The green lines (PIup and PIdown in the legend) indicate the prediction interval at a confidence level of 95%. The blue curve (pd in the legend) indicates the probability distribution of soil moisture soft data corresponding to the smallest value of temperature. (For interpretation of the references to color in this figure legend, the reader is referred to the web version of the article.)

Here, $\gamma(h)$ is the semivariance; $C_0$ represents a nugget, which is the minimum variability observed or the 'noise' at a distance of 0; $C_1$ is the structural variance, $C_0 + C_1$ represents the sill variance; a is the range that stands for the correlation length in geostatistics.

*Ordinary kriging, ordinary co-kriging and regression kriging*

Our study area is in the central part of the oasis, and no significant spatial trend of soil wetness can be found, so the soil moisture observations are assumed to meet the requirements of second-order stationarity for geostatistical inference and are assumed to be isotropic. The ordinary kriging (OK) estimator, as an optimally linear unbiased method, can be expressed as follows (Journel and Huijbregts, 1978):

$$Z^*(V_0) = \sum_{i=1}^{n} \lambda_i Z(V_i) \tag{6}$$

Optimal estimation requires the minimum variance of errors:

$$\sigma_k = Var\,[Z(v_0) - Z^*(v_0)] = E\left\{\left[Z(v_0) - \sum_{i=1}^{n}\lambda_i Z(v_i)\right]^2\right\} = \min \tag{7}$$

To ensure unbiased estimation, the following constraint condition must be added:

$$\sum_{i=1}^{n} \lambda_i = 1 \tag{8}$$

By applying the Lagrange Multiplier Method (LMM) with Eq. (7) as the object function and Eq. (8) as the constraint, and with the covariance information from the variogram, the weight coefficients $\lambda_i$ and Lagrange multiplier $\mu$ can be obtained, as can the optimal estimator $Z^*(v_0)$ and the estimation variance $\sigma_k$ (Journel and Huijbregts, 1978).

Similar to OK, the estimator of co-kriging (Co-OK) can be expressed as follows (Myers, 1982):

$$Z_1^*(v_0) = \sum_{i=1}^{n_1} \lambda_{1i} Z_1(v_{1i}) + \sum_{j=1}^{n_2} \lambda_{2j} Z_2(v_{2j}) \tag{9}$$

Eq. (10) provides optimal estimation, and as a result of the addition of a covariate to the estimator, another constraint condition, Eq. (12), has to be considered in addition to Eq. (11) to maintain unbiased estimation.

$$\sigma_c = Var\left[Z_1(v_0) - Z_1^*(v_0)\right]$$
$$= E\left\{\left[Z_1(v_0) - \sum_{i=1}^{n_1}\lambda_{1i}Z_1(v_{1i}) - \sum_{j=1}^{n_2}\lambda_{2j}Z_1(v_{2i})\right]^2\right\}$$
$$= \min \tag{10}$$

$$\sum_{i=1}^{n_1}\lambda_{1i} = 1 \tag{11}$$

$$\sum_{j=1}^{n_2}\lambda_{2j} = 1 \tag{12}$$

With the covariance information from the semivariance and cross-semivariance, the coefficients $\lambda_{1i}$ and $\lambda_{2j}$ can be obtained, as well as the estimator $Z_1^*(v_0)$ and the estimation variance $\sigma_c$ (Myers, 1982). Commonly, the primary variable and the covariate are positively or negatively correlated, and the absolute coefficient of correlation is greater than 0.5 (Asli and Marcotte, 1995). Of course, the covariate should be more intensively sampled, in which case the Co-OK method can be used in the most advantageous way. In this study, LST retrieved from remote sensing data can fully meet the requirements as an exhaustive covariate.

Regression kriging (RK) is an approach that combines a simple or multiple regression model with simple kriging of the regression residuals (Hengl et al., 2007). The regression predictions and residuals at all sampled locations were obtained by the regression, the experimental variogram of the residuals was computed and modeled, and the RK estimator is then written as the sum of the regression estimate and the kriged estimate of the spatially correlated residual values at $v_i$:

$$Z^*(v_0) = m^*(v_0) + \sum_{i=1}^{n}\lambda_i R(v_i) \tag{13}$$

where, $m^*(v_0)$ is the regression estimate for location $v_0$, and $R(v_i)$ are the residuals of the $n$ observation points, $R(v_i) = Z(v_i) - m(v_i)$. The estimation of optimal weights $\lambda_i$ can refer to the method of simple kriging. The linear regression model was introduced in Section "Preparation of soft data", and the experimental variogram of the residuals was computed and modeled in Section "Variogram and cross-variogram".

*Bayesian maximum entropy (BME)*

The concept of BME appeared more than two decades ago (Christakos, 1990b) and has been continuously developed and expanded (Christakos and Li, 1998; Christakos, 2000). BME introduces a theoretically sound and technically operational mapping method that makes it possible to incorporate measurements as well as various knowledge bases (soft data) in a logical manner (Christakos and Li, 1998). According to Christakos (2000), BME was generally introduced in the following three epistemological stages: a prior stage, a meta-prior stage, and a posterior stage. The general scheme of the method is depicted in Fig. 3.

The objective of the prior stage is to compute the joint pdf $f_G(x_{map})$, given general knowledge $G$, via the application of maximum entropy theory. The variable $x_{map}$ consists of a vector of points, $x_{soft}$, $x_{hard}$, and $x_k$, which denote the values of the soft and hard data points and unknown values at the estimation point, respectively. The expected information contained in the pdf can be expressed as Eq. (14) based on the Shannon information measure (Shannon and Weaver, 1948). The general knowledge $G$ in

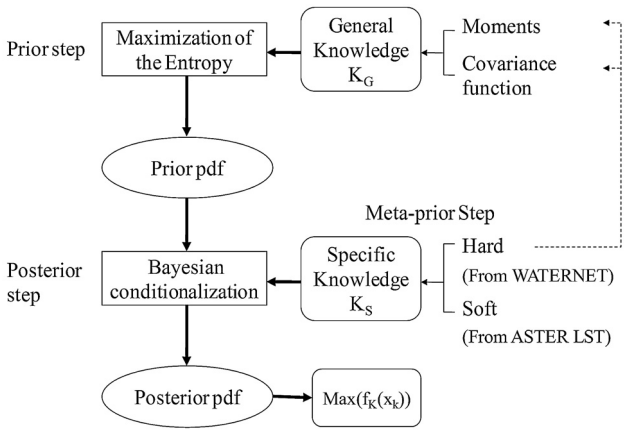


**Fig. 3.** Flowchart of the BME method.

Eq. (14) is expressed as $g_\alpha(x_{map})$, a set of functions of $x_{map}$ such as the mean and covariance moments. The shape of the prior pdf $f_G(x_{map})$ should be derived by means of a procedure that maximizes the expected information (Eq. (14)) and takes into consideration the constraints ($g_\alpha(x_{map})$), which represent general knowledge. Eq. (15) gives the object function of the Lagrange multipliers method (LMM) for maximizing the expected information by introducing the Lagrange multiplier $\mu_\alpha$. $E[g_\alpha(x_{map})]$ is the expected value of $g_\alpha(x_{map})$ (Christakos, 2000; Christakos and Li, 1998).

$$\overline{\text{Info}_G[x_{map}]} = -\int dx_{map} f_G(x_{map}) \log f_G(x_{map}) \tag{14}$$

$$M[f_G(x_{map})] = -\int dx_{map} f_G(x_{map}) \log f_G(x_{map}) - \sum_{\alpha}^{N}\mu_\alpha\left[\int g_\alpha f_G(x_{map}) f_G(x_{map}) dx_{map} - E[g_\alpha(x_{map})]\right] \tag{15}$$

At the meta-prior stage, new information is collected for the points to be estimated. This can include either specific sets of actual measurements (hard data) or soft data of various forms not considered at the prior stage (Christakos and Li, 1998). In this study, the soft data $f_S(x_{soft})$ were prepared in probability form, as detailed in Section "Preparation of soft data". At the posterior stage, the posterior pdf $f_K(x_k|x_{data})$ is expressed in terms of the prior pdf, the new data and information considered at the meta-prior stage as follows:

$$f_K(x_k|x_{data}) = A^{-1}\int dx_{soft} f_S(x_{soft}) f_G(x_{map}) \tag{16}$$

$$A = \int dx_{soft} f_S(x_{soft}) f_G(x_{data}) \tag{17}$$

Eq. (16) is a formulation of Bayes law, in which $x_{data}$ serves as a pointer for a context of knowledge, and $(x_k|x_{data})$ stands for the possible values $x_k$ of the map in the context specified by $x_{data}$. Hence, empirical knowledge is encoded in terms of the conditional pdf $f_K(x_k|x_{data})$ (Christakos and Li, 1998). From the posterior pdf $f_K(x_k|x_{data})$, two modes of estimator (mean in Eq. (18) and mode in Eq. (19)) can be used:

$$x_k^* = \int x_k f_k(x_k|x_{data}) dx_k \tag{18}$$

$$x_k^* = \max(f_K(x_k|x_{data})) \tag{19}$$

Here, $x_k^*$ is the estimation of $x_k$. In this study, the estimator of Eq. (19) was employed. A more detailed discussion of the epistemic principles and mathematical analysis leading to the BME formulas above may be found in Christakos and Li (1998) and Christakos (2000). The BMElib library (Christakos et al., 2002) is helpful for implementing the method. Note that the covariance function was needed in BME to provide the spatial covariance. Under the hypothesis of second order stationary, we can obtain the following relationship between the variogram and the covariance function: $C(h) = sill - \gamma(h)$ (Schabenberger and Gotway, 2004). Thus, the covariance function can be obtained simply based on the variogram modeled in Section "Variogram and cross-variogram". What also should be noticed is that the auxiliary data (ASTER LST) can be useful only in the three periods introduced above, so the BME method in this study was only tested in the case of spatial estimation, even though BME can also provide excellent performance in the spatiotemporal analysis.

*Methods of validation*

In this study, the presentation of the spatial estimation is evaluated by two strategies. One strategy is a commonly used method of cross-validation, and the other is validation by an extra dataset that we define as absolute validation. The extra dataset was composed of the soil moisture observations from the auto weather station (AWS). Additionally, the following three statistical indicators (Eqs. (20)–(22)) are used to quantitatively evaluate the accuracy of the results: root-mean-squared error (RMSE), correlation coefficient (CR), and mean bias (bias).

$$\mathrm{RMSE} = \sqrt{\sum_{k=1}^{n} \frac{(x_k^* - x_k)^2}{n}} \tag{20}$$

$$\mathrm{CR} = \frac{\sum_{k=1}^{n}(x_k^* - \bar{x}^*)(x_k - \bar{x})}{\sqrt{\sum_{k=1}^{n}(x_k^* - \bar{x}^*)^2}\sqrt{\sum_{k=1}^{n}(x_k - \bar{x})^2}} \tag{21}$$

$$\mathrm{Bias} = \frac{\sum_{k=1}^{n}(x_k^* - x_k)}{n} \tag{22}$$

## Results and discussion

*Variogram and cross-variogram analysis*

The semivariance of SM, residual, LST, and the cross-semivariance are shown in Fig. 4 as a function of spatial lag $h$. The experimental semivariance values are shown with circle-marked scatters, and the theoretical models fit to the scatters are displayed as black curves. Table 4 shows all of the parameters of the fitted theoretical models. In most cases, model (1) was preferred. Model (2) was used only for the cross-variogram on May30, 2012. $R^2$ in Table 4, especially for models of the covariates, are all large enough to indicate that the theoretical model represents the actual semivariance well. Here, $C_0$ and $C_0 + C_1$ for the cross-variograms were negative because of the negative correlation between SM and LST. The sill variances ($C_0 + C_1$) of SM for May 30, 2012 and June 24, 2012 are relatively larger compared to that of June 15, 2012, which shows that the spatial variation of SM is greater on May 30, 2012 and June 24, 2012 than on June 15, 2012. Although it was moderately correlated with SM, LST on June 24, 2012 did not show high spatial variation (sill variance) as on May 30, 2012. This may be due to the heavier vegetation cover on June 24, 2012, which has more of an effect on LST of ASTER. Generally, it was also noted that the residual variogram have approximately the same form and nugget but a somewhat smaller sill and range. The range for variograms of SM, LST, and the cross in the same period are basically similar, it is approximately 1800 m for May 30, 2012, approximately 1500 m for June 24, 2012, and approximately 1100 m for June15, 2012. In all three periods, the semivariance and the cross-semivariance obey the Cauchy-Schwartz inequality mentioned above.

*Spatial estimation of soil moisture*

The spatial distribution of soil moisture in the study area was estimated at a resolution of 90 m by the four methods introduced previously. The methods were implemented in the programming environment of MATLAB. We suppose that the soil moisture in each pixel area of the estimation map is homogeneous, so the pixel value is represented by the estimation value of the pixel center point.

Fig. 5 shows the soil moisture distribution map of the study area in the three periods obtained by the four methods. The white areas in the maps represent the masked areas of buildings that appear just like islands and have no correlation with the surrounding environment. In each period (each column of Fig. 5), the spatial structure of soil moisture for all four methods is generally similar, and they even provided a similar changing range of wetness. Obviously, a larger spatial variation of wetness occurred globally on May 30, 2012 and June 24, 2012, but the wetness appears to be more homogeneous on June 15, 2012. Locally speaking, the change in the map of OK is smooth, whereas the grid phenomenon is clearer in Co-OK and RK. Compared with OK and Co-OK, the RK and BME map exhibits more spatial variation information, especially in the border region of the study area where the point observations are relatively sparse. Visual comparisons of the estimation results can only provide preliminary realizations about the spatial distribution of soil moisture. For the presentation of each estimation method, quantitative validation work is also necessary. We discuss this work in the following section.

*Cross-validation*

After the generation of a soil moisture distribution map, cross-validation was applied (leave-one-out method). In the cross-validation, $x_k^*$ is defined as the estimated soil moisture at a location where the actual value $x_k$ was available but removed prior to spatial estimation. Thus, the cross-validation error can be defined as $(x_k^* - x_k)$. Figs. 6–8 show scatter plots and error distributions of cross-validation in the three experimental periods. Table 5 contains the corresponding statistical indicators.

From the indicator of Bias in Table 5, we can see that all the methods provide excellent unbiased estimations. The CR of Co-OK is only slightly larger than that of OK, but both of which show moderate correlation between the estimations and observations on May 30, 2012 and June 24, 2012, and even show low correlation on June 15, 2012, however the majority of scatters are located around the 1:1 line, according to Fig. 6. Additionally, we can find that the CR for both RK and BME are obviously larger than that of Co-OK. The CR of RK can reach 0.61 on May 30, 2012, CR of BME can reach can reach 0.71 on June 24, 2012 and even 0.76 on May 30, 2012, and CR of BME are large than that of RK in the mass. RMSE of SM predicted by OK ranged from 0.0447 to 0.0645 $m^3/m^3$ in the three periods, by contrast the other three methods which integrated the auxiliary data can all provide more accurate estimation, especially the BME method, and the RMSE of which is obviously smaller than others. All of above data suggest that Co-OK can slightly outperform OK even though also integrated the LST information, both RK and BME can incorporate the information of LST more efficiently than Co-OK, and BME can perform better than RK.

According to the distribution of scatters and the histogram in Figs. 6–8, the methods all provide reasonable estimation for a majority of the validation points. There are relatively large errors in only a few points, which may be due to regional spatial correlation

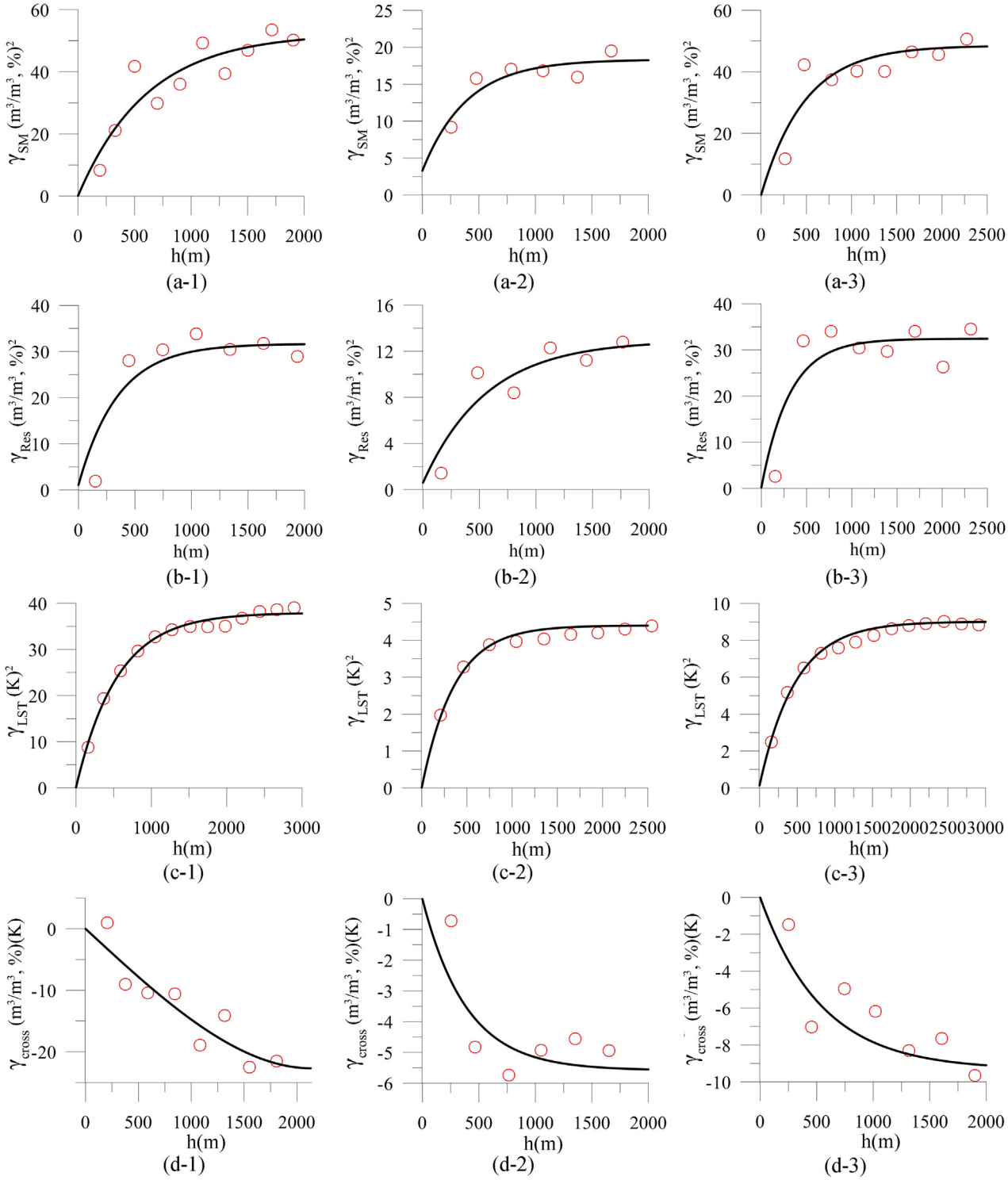


**Fig. 4.** Experimental and fitted theoretical variograms. (a-1), (b-1), (c-1) and (d-1) are respectively variograms of SM, residual, LST and the cross between SM and LST on May 30, 2012. (a-2), (b-2), (c-2) and (d-2) are for June 15, 2012, and (a-3), (b-3), (c-3) and (d-3) are for June 24, 2012.

that cannot be fully represented by the under-sampled hard data in this study. The error histograms also show that the error range was reduced in each experimental period if the auxiliary data were integrated, especially in the case of BME. Similar to the inherent disadvantage of OK (Kravchenko, 2008), Co-OK, RK and BME may also overestimate in the range of low values and underestimate in the range of high values, but this can be improved in RK and BME even when the soil moisture and the covariate LST are moderately correlated as in this study.

*Validation by soil moisture observations from auto-weather stations (AWS)*

In addition to cross-validation, we carried out absolute validation work for each method by using the soil moisture observations of AWS, which were absolutely not used in the spatial estimation. Because fewer than 10 AWSs are normally running, only those stations can provide soil moisture observations for each period are used. Here, we treated the validation data in the three

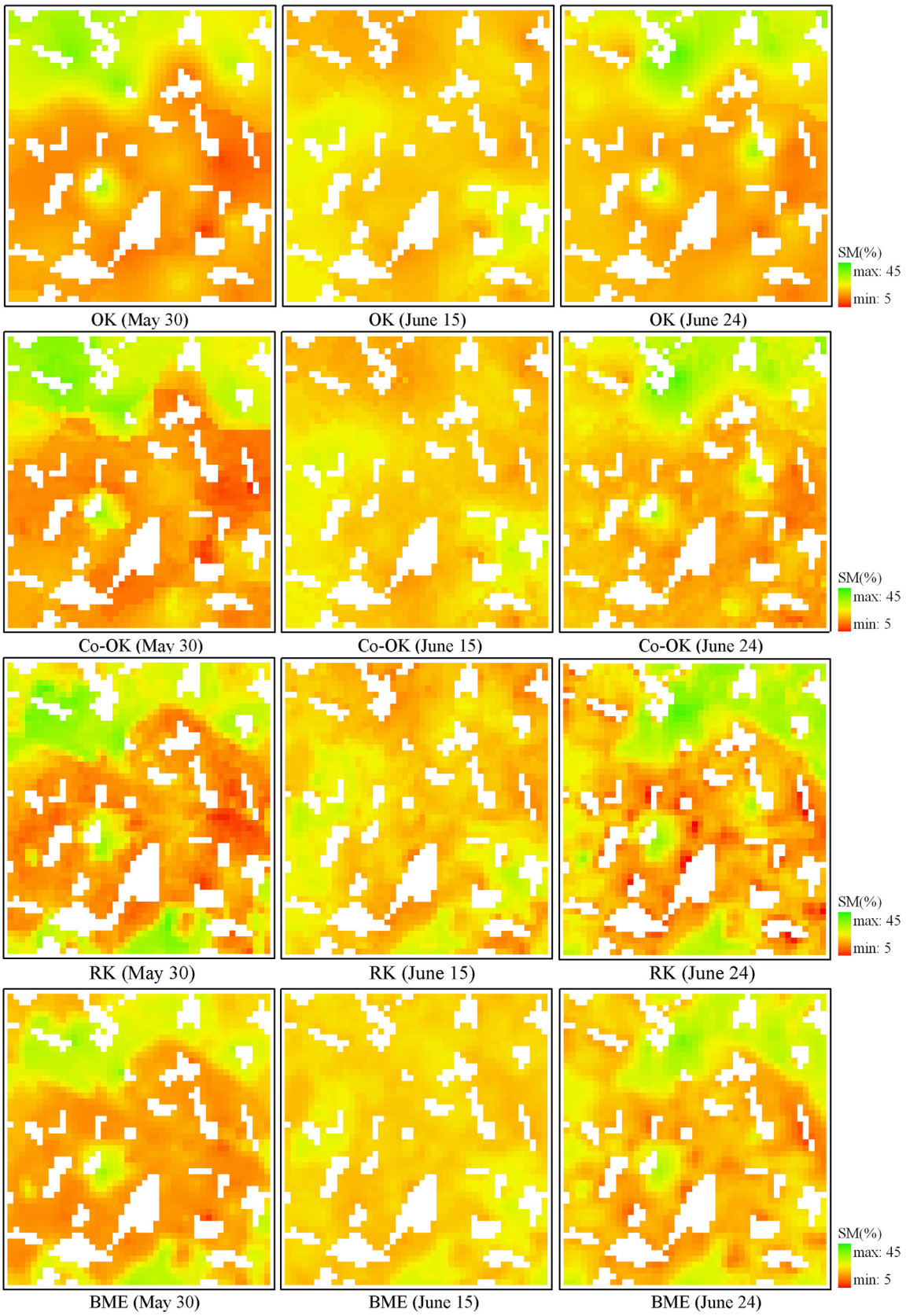


**Fig. 5.** Spatial distribution of soil moisture estimated by OK, Co-OK, RK and BME. The first column includes the estimation results of the four methods on May 30, 2012, the second column is for June 15, 2012 and the third column is for June 24, 2012. The white areas in each map stand for the masked areas.

**Table 4**
Parameters of variogram and cross-variogram models.

| Date | Variable | Variogram model | $C_0$ | $C_0 + C_1$ | $a$ (m) | $R^2$ |
|---|---|---|---|---|---|---|
| May 30 | Soil moisture | Model (1) | 0.1 (a) | 52.29 (a) | 1836 | 0.817 |
| May 30 | Residual | Model (1) | 1.1 (a) | 30.59 (a) | 1047 | 0.537 |
| May 30 | LST | Model (1) | 0.1 (b) | 37.86 (b) | 1638 | 0.988 |
| May 30 | Cross | Model (2) | −0.01 (c) | −22.68 (c) | 2139 | 0.845 |
| June 15 | Soil moisture | Model (1) | 3.3 (a) | 18.35 (a) | 1180 | 0.794 |
| June 15 | Residual | Model (1) | 0.6 (a) | 12.34(a) | 1692 | 0.672 |
| June 15 | LST | Model (1) | 0.01 (b) | 4.393 (b) | 1086 | 0.922 |
| June 15 | Cross | Model (1) | −0.01 (c) | −5.575 (c) | 1167 | 0.642 |
| June 24 | Soil moisture | Model (1) | 0.1 (a) | 48.52 (a) | 1452 | 0.763 |
| June 24 | Residual | Model (1) | 0.2 (a) | 32.23(a) | 945 | 0.491 |
| June 24 | LST | Model (1) | 0.14 (b) | 8.876 (b) | 1434 | 0.989 |
| June 24 | Cross | Model (1) | −0.01 (c) | −9.33 (c) | 1638 | 0.709 |

*Note*: a, stands for $(m^3/m^3)^2$; b, stands for $K^2$; c, stand for $(m^3/m^3)$*K.

**Table 5**
Summary statistics of cross-validation.

| Date | No. of WSN | Method | Covariate | CR | RMSE (%) | Bias (%) |
|---|---|---|---|---|---|---|
| May 30 | 47 | OK | N | 0.54 | 6.28 | −0.19 |
| May 30 | 47 | Co-OK | Y | 0.61 | 6.08 | 0.07 |
| May 30 | 47 | RK | Y | 0.62 | 6.02 | 0.04 |
| May 30 | 47 | BME | Y | 0.76 | 5.01 | −0.05 |
| June 15 | 45 | OK | N | 0.20 | 4.47 | 0.20 |
| June15 | 45 | Co-OK | Y | 0.21 | 4.37 | 0.11 |
| June15 | 45 | RK | Y | 0.45 | 3.97 | 0.15 |
| June 15 | 45 | BME | Y | 0.62 | 3.42 | −0.05 |
| June 24 | 42 | OK | N | 0.43 | 6.45 | −0.12 |
| June 24 | 42 | Co-OK | Y | 0.45 | 6.38 | −0.22 |
| June 24 | 42 | RK | Y | 0.55 | 6.04 | −0.19 |
| June 24 | 42 | BME | Y | 0.71 | 5.21 | 0.04 |

*Note:* Y, denotes using the covariate; N, not using the covariate; units for RMSE and Bias are $m^3/m^3$.

periods (29 points total) as one statistical data base. Fig. 9 shows the scatters between the observed SM of AWS and the SM estimated by OK, Co-OK, RK and BME. The same statistical indicators used in cross-validation were calculated and are listed in Table 6. Similar to cross-validation, we found that Co-OK, even though it incorporated the ASTER LST, did not exhibit evident improvement compared with OK. The moderate correlation between the target variable (SM) and the covariate (ASTER LST) in this study may have limited the improvement of the accuracy because Co-OK does not use physically interpretable relationships between the target variable (SM) and auxiliary variable (LST), but rather assumes a linear relationship in the estimator. This finding is consistent with previous

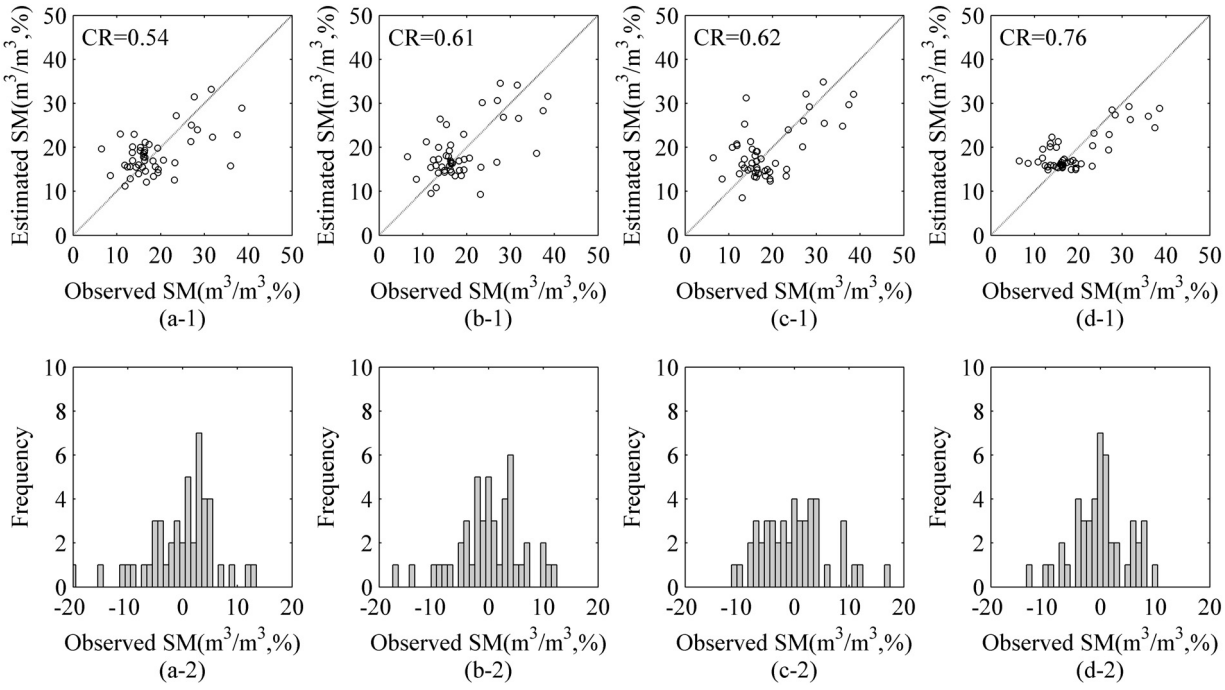


**Fig. 6.** Cross-validation and error distribution for OK, Co-OK, RK and BME on May 30, 2012. (a-1), (a-2) are for OK, (b-1), (b-2) are for Co-OK, (c-1), (c-2) are for RK, and (d-1), (d-2) are for BME.

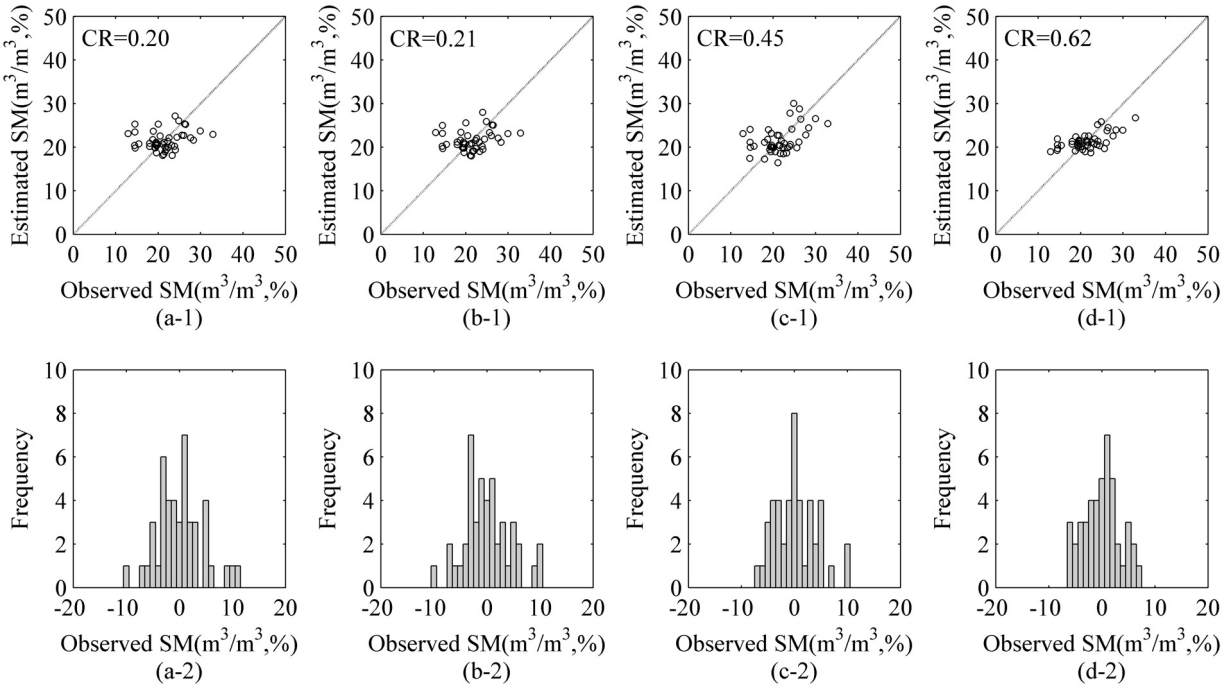


**Fig. 7.** Cross-validation and error distribution for OK, Co-OK, RK and BME on June 15, 2012. (a-1), (a-2) are for OK, (b-1), (b-2) are for Co-OK, (c-1), (c-2) are for RK, and (d-1), (d-2) are for BME.

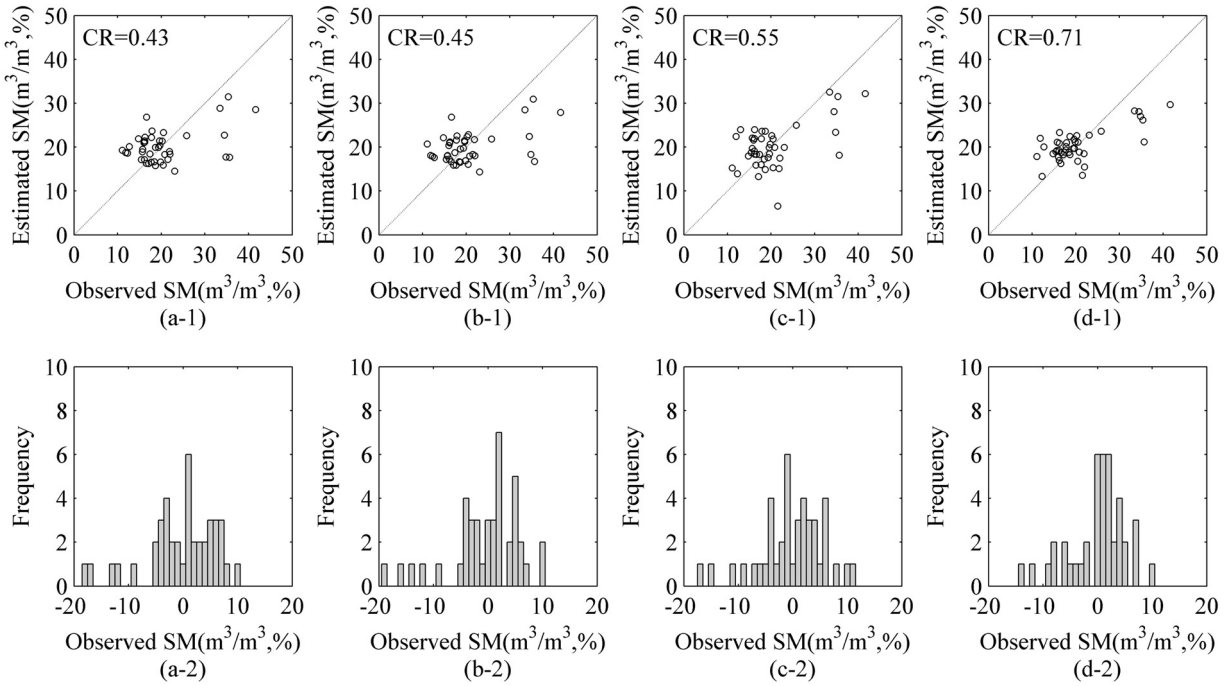


**Fig. 8.** Cross-validation and error distribution for OK, Co-OK, RK and BME on June 24, 2012. (a-1), (a-2) are for OK, (b-1), (b-2) are for Co-OK, (c-1), (c-2), are for RK and (d-1), (d-2) are for BME.

**Table 6**
Summary statistics of validation by AWS.

| Date | No. of points | Method | Covariate | CR | RMSE (%) | Bias (%) |
|---|---|---|---|---|---|---|
| May 30, June 15, June 24 | 29 | OK | N | 0.27 | 5.61 | −0.14 |
| May 30, June 15, June 24 | 29 | Co-OK | Y | 0.28 | 5.51 | −0.15 |
| May 30, June 15, June 24 | 29 | RK | Y | 0.60 | 3.92 | −0.07 |
| May 30, June 15, June 24 | 29 | BME | Y | 0.68 | 3.86 | −0.07 |

*Note*: Y, denotes using the covariate; N, not using the covariate; units for RMSE and Bias are $m^3/m^3$.

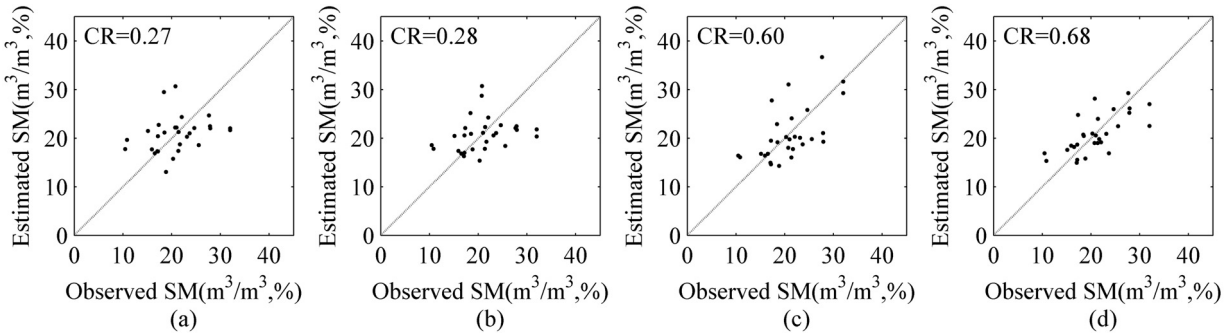


**Fig. 9.** The observed SM of AWSs versus estimated SM by OK, Co-OK, RK and BME. (a) is for OK, (b) is for Co-OK, (c) is for RK, and (d) is for BME.

conclusions that Co-OK can underweight the covariates and shows only minimally superiority to OK when the auxiliary variables are not highly correlated with the primary variable (Goovaerts, 1998; Triantafilis et al., 2001; Wu et al., 2009; Emery, 2012).

Both RK and BME show noticeable advantages over OK and Co-OK in the absolute validation. The CR reached 0.60 for RK and 0.68 for BME. The RMSE of RK reduced to 0.0392 $m^3/m^3$ from 0.0551 $m^3/m^3$ of Co-OK, even more, the RMSE of BME can reduced to 0.0386 $m^3/m^3$. Additionally, the CR of and RK and BME are greater than that of the linear regression shown in Table 3, which indicates that RK and BME can more fully incorporate the valuable information from target variables and uncertain auxiliary variables, and BME even performs better than RK.

Although the issue of overestimation in the range of low values and underestimation in the range of high values still exists in BME, RK and Co-OK, it can be improved compared to OK, especially in BME and OK as show in Fig. 9. We can say that the auxiliary information (LST) incorporated into the estimation by Co-OK, RK and BME plays an important role here. We also expect that integrating two or more covariates and more highly correlated auxiliary data may also provide a solution for the issue, so the strength of the relationship between the target variable and the auxiliary variable is important for choosing the auxiliary data. Nevertheless, the problems (overestimation and underestimation) in absolute validation by AWSs seem less important than those of the cross-validation according to the scatter diagrams of absolute validation and cross-validation. It is noted that partial error may be introduced by the cross-validation method itself in the under-sampled cases. For example, the extreme values (max or min) of the observations may be highly representative of the local area, if they are left out as the validation data, the observations used in the estimator of the points (where the extreme observations occurred) cannot fully reproduce or predict the extreme values. This will lead to an extra component of error and aggravate the issue of overestimation of high values and underestimation of low values. Thus, validation by use of extra data was suggested in the spatial estimation.

## Conclusions

The large spatial variation of the land surface soil moisture and the commonly under-sampled soil moisture in situ (network) data make the spatially accurate estimation of soil moisture an arduous task. This study focused on the spatial estimation of soil moisture by integrating auxiliary information from ASTER LST. The spatial analysis method BME was introduced here. For comparison, the OK method, which uses only hard data, and Co-OK and RK methods, which also incorporates auxiliary information, were also carried out in the study. In BME, linear regression was first used to retrieve soil moisture directly from the ASTER LST, and the *t*-distributed PI was estimated and expressed as probability soft data. Based on this study, we can indeed conclude that integrating the auxiliary data (LST) in the spatial estimation of soil moisture can improve the estimation accuracy. Co-OK did not show evident improvement over the results of OK. In contrast, RK and BME can more fully fuse the valuable information from target variables and auxiliary variables, even the BME method can performs slightly better than RK. The estimation accuracy and the inherent issue of spatial estimation (overestimation in the range of low values and underestimation in the range of high values) are both obviously improved in RK and BME. Moreover, integrating highly correlated auxiliary data can also be a potential solution of the inherent issue, so the strength of the relationship between the target variable and the auxiliary variable is important for choosing auxiliary data. It is also noted that partial error may be introduced by the cross-validation method itself in under-sampled cases, so validation by an extra data was suggested. In general, BME has greater potential to successfully fuse the uncertain auxiliary data in spatial estimation, and it can further improve the estimation accuracy of soil moisture even in under-sampled cases. Moreover, using an appropriate auxiliary variable is important for obtaining successful spatial estimation results for soil moisture.

## Conflict of interest statement

We declare that we have no financial and personal relationships with other people or organizations that can inappropriately influence our work, there is no professional or other personal interest of any nature or kind in any product, service and/or company that could be construed as influencing the position presented in the manuscript entitled “Estimating the spatial distribution of soil moisture based on Bayesian maximum entropy method with auxiliary data from remote sensing”.

## Acknowledgments

The authors thank the anonymous reviewers of this paper for providing constructive comments which have contributed greatly to improve the final version. Also, we thank all of the scientists, engineers and students who participated in the HiWATER field campaigns. This work was funded by the National Natural Science Foundation of China (91125002 and 41071225) and the National High Technology Research and Development Program (2012AA12A305). We also greatly thank the BMElab of University of North Carolina at Chapel Hill for sharing the program package BMElib.

## References

Akyildiz, I.F., Su, W., Sankarasubramaniam, Y., Cayirci, E., 2002. Wireless sensor networks: a survey. Comput. Netw. 38, 393–422.
Asli, M., Marcotte, D., 1995. Comparison of approaches to spatial estimation in a bivariate context. Math. Geol. 27, 641–658.

Bartlett, J.E., Kotrlik, J.W., Higgins, C.C., 2001. Organizational research: Determining appropriate sample size in survey research appropriate sample size in survey research. Inf. Technol. Learn. Perform. J. 19 (1), 43–50.

Bogaert, P., D'Or, D., 2002. Estimating soil properties from thematic soil maps. Soil Sci. Soc. Am. J. 66, 1492–1500.

Bogaert, P., Christakos, G., Jerrett, M., Yu, H.L., 2009. Spatiotemporal modelling of ozone distribution in the State of California. Atmos. Environ. 43, 2471–2480.

Bogena, H.R., Herbst, M., Huisman, J.A., Rosenbaum, U., Weuthen, A., Vereecken, H., 2010. Potential of wireless sensor networks for measuring soil water content variability. Vadose Zone J. 9, 1002–1013.

Boyer, D.G., Wright, R.J., Feldhake, C.M., Bligh, D.P., 1996. Soil spatial variability relationships in a steeply sloping acid soil environment. Soil Sci. 161, 278–287.

Burgess, T., Webster, R., 1980. Optimal interpolation and isarithmic mapping of soil properties. J. Soil Sci. 31, 333–341.

Cheng, G.D., 2009. Integrated Management of the Water-Ecology-Economy System in the Heihe River Basin. Science Press, Beijing (in Chinese).

Christakos, G., 1990a. A Bayesian/maximum-entropy view to the spatial estimation problem. Math. Geol. 22, 763–776.

Christakos, G., 1990b. Modern Spatiotemporal Geostatistics. Oxford University Press, New York.

Christakos, G., 1991. Some Applications of the Bayesian, Maximum-Entropy Concept in Geostatistics. Maximum Entropy and Bayesian Methods. Springer, Netherlands.

Christakos, G., Li, X., 1998. Bayesian maximum entropy analysis and mapping: a farewell to kriging estimators? Math. Geol. 30, 435–462.

Christakos, G., 2000. Modern Spatiotemporal Geostatistics. Oxford University Press, New York.

Christakos, G., Serre, M.L., 2000. BME analysis of spatiotemporal particulate matter distributions in North Carolina. Atmos. Environ. 34, 3393–3406.

Christakos, G., Serre, M.L., Kovitz, J.L., 2001. BME representation of particulate matter distributions in the state of California on the basis of uncertain measurements. J. Geophys. Res. Atmos. 106, 9717–9731.

Christakos, G., Bogaert, P., Serre, M.L., 2002. Temporal GIS. Springer-Verlag, New York.

Christakos, G., Kolovos, A., Serre, M.L., Vukovich, F., 2004. Total ozone mapping by integrating data bases from remote sensing instruments and empirical models. IEEE Trans. Geosci. Remote 42, 991–1008.

Cressie, N., 1990. The origins of kriging. Math. Geol. 22, 239–252.

D'Or, D., (Ph.D. dissertation) 2003. Spatial Prediction of Soil Properties, the Bayesian Maximum Entropy Approach. Université catholique de Louvain, Louvain, Belgium.

D'Or, D., Bogaert, P., Christakos, G., 2001. Application of the BME approach to soil texture mapping. Stoch. Environ. Res. Risk Assess. 15, 87–100.

Douaik, A., Meirvenne, M., Toth, T., 2004. Space–time mapping of soil salinity using probabilistic Bayesian maximum entropy. Stoch. Environ. Res. Risk Assess. 18, 219–227.

Douaik, A., Van, M.M., Tóth, T., 2005. Soil salinity mapping using spatio-temporal kriging and Bayesian maximum entropy with interval soft data. Geoderma 128, 234–248.

Emery, X., 2012. Cokriging random fields with means related by known linear combinations. Comput. Geosci. 38, 136–144.

Entekhabi, D., Njoku, E.G., O'Neill, P.E., Kellogg, K.H., Crow, W.T., Edelstein, W.N., Van, Z.J., 2010. The soil moisture active passive (SMAP) mission. Proc. IEEE 98, 704–716.

Goovaerts, P., 1998. Ordinary cokriging revisited. Math. Geol. 30, 21–42.

Goovaerts, P., 1999. Using elevation to aid the geostatistical mapping of rainfall erosivity. Catena 34 (3), 227–242.

Guswa, A.J., Celia, M.A., Rodriguez-Iturbe, I., 2002. Models of soil moisture dynamics in ecohydrology: a comparative study. Water Resour. Res. 38, 5-1–5-15.

Hengl, T., Heuvelink, G., Rossiter, D.G., 2007. About regression-kriging: from equations to case studies. Comput. Geosci. 33 (10), 1301–1315.

Hernández-Stefanoni, J.L., Alberto Gallardo-Cruz, J., Meave, J.A., et al., 2011. Combining geostatistical models and remotely sensed data to improve tropical tree richness mapping. Ecol. Ind. 11 (5), 1046–1056.

Hu, Y.Q., Gao, Y.X., Wang, J.M., Ji, G.L., Shen, Z.B., Cheng, L.S., Chen, J.Y., Li, S.Q., 1994. Some achievements in scientific research during HEIFE. Plateau Meteorol. 13, 225–236 (in Chinese).

Jackson, T., Bindlish, R., Cosh, M., 2009. Validation of AMSR-E soil moisture products using in-situ observations. J. Remote Sens. Soc. Japan 29, 263–270.

Jackson, T., Cosh, M., Crow, W., Colliander, A., Walker, J., 2011. In situ validation of the Soil Moisture Active Passive (SMAP) satellite mission. In: 34th International Symposium on Remote Sensing of Environment, Sydney, Australia.

Jin, R., Li, X., Yan, B., 2012. Introduction of eco-hydrological wireless sensor network in the Heihe River Basin. Adv. Earth Sci. 27, 993–1005 (in Chinese).

Journel, A.G., Huijbregts, C.J., 1978. Mining Geostatistics. Academic Press, London.

Kerr, Y.H., Waldteufel, P., Wigneron, J., Delwart, S., Cabot, F., Boutin, J., Escorihuela, M., Font, J., Reul, N., Gruhier, C., Juglea, S.E., Drinkwater, M.R., Hahne, A., Martín-Neira, M., Mecklenburg, S., 2010. The SMOS mission: new tool for monitoring key elements of the global water cycle. Proc. IEEE 98, 666–687.

Knotters, M., Brus, D.J., Oude Voshaar, J.H., 1995. A comparison of kriging, co-kriging and kriging combined with regression for spatial interpolation of horizon depth with censored observations. Geoderma 67 (3), 227–246.

Kravchenko, A.N., 2008. Stochastic simulations of spatial variability based on multifractal characteristics. Vadose Zone J. 7, 521–524.

Lakshmi, V., Zehrfuhs, D., Jackson, T., 2000. Observations of land surface temperature and its relationship to soil moisture during SGP99. In: Proc. IGARSS. 3, pp. 1256–1258.

Le Vine, D.M., Lagerloef, G.S., Torrusio, S.E., 2010. Aquarius and remote sensing of sea surface salinity from space. Proc. IEEE 98, 688–703.

Lee, S.J., (Ph.D. dissertation) 2005. Models of Soft Data in Geostatistics and their Application in Environmental and Health Mapping. Univ. of N. C. at Chapel Hill.

Lee, S., Yeatts, K., Serre, L.M., 2009. A Bayesian maximum entropy approach to address the change of support problem in the spatial analysis of childhood asthma prevalence across North Carolina. Spatial Spatio-temporal Epidemiol. 1, 49–60.

Li, A., Bo, Y., Chen, L., 2012. Bayesian maximum entropy data fusion of field-observed leaf area index (LAI) and Landsat Enhanced Thematic Mapper Plus-derived LAI. Int. J. Remote Sens. 34, 227–246.

Li, A., Bo, Y., Zhu, Y., Guo, P., Bi, J., He, Y., 2013a. Blending multi-resolution satellite sea surface temperature (SST) products using Bayesian maximum entropy method. Remote Sens. Environ. 135, 52–63.

Li, X., Li, X.W., Li, Z.Y., Ma, M.G., Wang, J., Xiao, Q., Liu, Q., Ren, H.Z., 2009. Watershed allied telemetry experimental research. J. Geophys. Res. 114, D22.

Li, X., Cheng, G.D., Liu, S.M., Xiao, Q., Ma, M.G., Jin, R., Xu, Z.W., 2013b. Heihe Watershed Allied Telemetry Experimental Research (HiWATER): scientific objectives and experimental design. Bull. Am. Meteorol. Soc. 94, BAMS-D-12-00154.

Moral, F.J., 2010. Comparison of different geostatistical approaches to map climate variables: application to precipitation. Int. J. Climatol. 30 (4), 620–631.

Myers, D.E., 1982. Matrix formulation of co-kriging. Math. Geol. 14, 249–257.

Nazelle, D.A., Arunachalam, S., Serre, L.M., 2010. Bayesian maximum entropy integration of ozone observations and model predictions: an application for attainment demonstration in North Carolina. Environ. Sci. Technol. 44, 5707–5713.

Ottlé, C., Stoll, M., 1993. Effect of atmospheric absorption and surface emissivity on the determination of land surface temperature from infrared satellite data. Int. J. Remote Sens. 14 (10), 2025–2037.

Pang, W., Christakos, G., Wang, J.F., 2010. Comparative spatiotemporal analysis of fine particulate matter pollution. Environmetrics 21, 305–317.

Rivero, R.G., Grunwald, S., Bruland, G.L., 2007. Incorporation of spectral data into multivariate geostatistical models to map soil phosphorus variability in a Florida wetland. Geoderma 140 (4), 428–443.

Ruiz-Garcia, L., Lunadei, L., Barreiro, P., Robla, I., 2009. A review of wireless sensor technologies and applications in agriculture and food industry: state of the art and current trends. Sensors 9, 4728–4750.

Schabenberger, O., Gotway, C.A., 2004. Statistical Methods for Spatial Data Analysis. Chapman and Hall/CRC Press.

Serre, M.L., Christakos, G., 1999. Modern geostatistics: computational BME in the light of uncertain physical knowledge-The Equus Beds study. Stoch. Environ. Res. Risk Assess. 13 (1/2), 1–26.

Shannon, C.E., Weaver, W., 1948. A mathematical theory of communication. Bell Syst. Technol. J. 7, 379–423.

Stein, A., Corsten, L.C.A., 1991. Universal kriging and cokriging as a regression procedure. Biometrics, 575–587.

Stein, A., Van, D.W., Bouma, J., Bregt, A.K., 1988. Cokriging point data on moisture deficit. Soil Sci. Soc. Am. J. 52, 1418–1423.

Sun, D., Pinker, R.T., 2004. Case study of soil moisture effect on land surface temperature retrieval. IEEE Geosci. Remote Sens. Lett. 1, 127–130.

Triantafilis, J., Odeh, I.O.A., McBratney, A.B., 2001. Five geostatistical models to predict soil salinity from electromagnetic induction data across irrigated cotton. Soil Sci. Soc. Am. J. 65, 869–878.

Vereecken, H., Huisman, J.A., Bogena, H.R., Vanderborght, J., Vrugt, J.A., Hopmans, J.W., 2008. On the value of soil moisture measurements in vadose zone hydrology: a review. Water Resour. Res. 44, W00D06.

Wang, L., Qu, J.J., 2009. Satellite remote sensing applications for surface soil moisture monitoring: a review. Front. Earth Sci. China 3, 237–247.

Wu, C., Wu, J., Luo, Y., Zhang, L., DeGloria, S.D., 2009. Spatial prediction of soil organic matter content using cokriging with remotely sensed data. Soil Sci. Soc. Am. J. 73, 1202–1208.

Wu, J., Norvell, W.A., Hopkins, D.G., Smith, D.B., Ulmer, M.G., Welch, R.M., 2003. Improved prediction and mapping of soil copper by kriging with auxiliary data for cation-exchange capacity. Soil Sci. Soc. Am. J. 67, 919–927.

Yates, S.R., Warrick, A.W., 1987. Estimating soil water content using cokriging. Soil Sci. Soc. Am. J. 51, 23–30.

Younger, M.S., 1985. A First Course in Linear Regression, 2nd ed. Duxbury Press, Boston.

Yu, H.L., Chen, J.C., Christakos, G., Jerrett, M., 2009. BME estimation of residential exposure to ambient PM10 and ozone at multiple time scales. Environ. Health Perspect. 117, 537–544.

Zhang, R.D., Myers, D.E., Warrick, A.W., 1992. Estimation of the spatial distribution of soil chemicals using pseudo-cross-variograms. Soil Sci. Soc. Am. J. 56, 1444–1452.

Zhang, R.D., Shouse, P., Yates, S., 1997. Use of pseudo-crossvariograms and cokriging to improve estimates of soil solute concentrations. Soil Sci. Soc. Am. J. 61, 1342–1347.

Zhang, R.D., 2005. Theory and Application of Spatial Variation. Science Press, Beijing (in Chinese).

Zhou, J., Li, J., Zhang, L., Hu, D., Zhan, W., 2012. Intercomparison of methods for estimating land surface temperature from a Landsat-5 TM image in an arid region with low water vapour in the atmosphere. Int. J. Remote Sens. 33, 2582–2602.